# Photofragment Imaging Differentiates Between One and Two-Photon Dissociation Pathways in $MgI^+$

Schuyler P. Lockwood and Ricardo B. Metz*
*Department of Chemistry, University of Massachusetts Amherst*

email: rbmetz@chem.umass.edu
Phone: +1-413-545-6089. Fax: +1-413-545-4490

## Abstract

The bond strength and photodissociation dynamics of $MgI^+$ are determined by a combination of theory, photodissociation spectroscopy and photofragment velocity map imaging. From 17000 to 21500 $cm^{-1}$ the photodissociation spectrum of $MgI^+$ is broad and unstructured; photofragment images in this region show perpendicular anisotropy, consistent with absorption to the repulsive wall of the (1) $\Omega$=1 or (2) $\Omega$=1 states followed by direct dissociation to ground state products $Mg^+$ ($^2S$) + I ($^2P_{3/2}$). Analysis of photofragment images taken at photon energies near threshold gives a bond dissociation energy $D_0(Mg^+\text{-}I)$ = 203.0 ± 1.8 kJ/mol (2.10 ± 0.02 eV; 17000 ± 150 $cm^{-1}$). At photon energies of 33000 to 41000 $cm^{-1}$, exclusively $I^+$ fragments are formed. Over most of this region, formation of $I^+$ is not energetically allowed via one-photon absorption from the ground state of $MgI^+$. Images show the observed products result from resonance enhanced two-photon dissociation. The photodissociation spectrum from 33000 to 38500 $cm^{-1}$ shows vibrational structure, giving an average excited state vibrational spacing of 227 $cm^{-1}$. This is consistent with absorption to the (3) $\Omega=0^+$ state from v=0, 1 of the (1) $\Omega=0^+$ ground state; from the (3) $\Omega=0^+$ state, absorption of a second photon results in dissociation to Mg* ($^3P_J^\circ$) + $I^+$ ($^3P_J$). From 38500 to 41000 $cm^{-1}$ the spectrum is broad and unstructured. We attribute this region of the spectrum to one-photon dissociation of vibrationally hot $MgI^+$ at low energy and ground state $MgI^+$ at higher energy, to form Mg ($^1S$) + $I^+$ ($^3P_J$) products.

## I. Introduction

Interactions and reactions within alkali and alkaline earth metal ion – ligand complexes have been studied by a wide variety of mass spectrometric techniques as they can be dissociated by collisions or, by taking advantage of their strongly absorbing atomic transitions in the visible and UV, can be probed by photodissociation, or "half-collisions". Magnesium cation ($Mg^+$) complexes have received significant attention by groups employing the latter method with laser photolysis near the 280 nm $Mg^+$ $^2P_{1/2,\ 3/2} \leftarrow {}^2S_{1/2}$ (*3p* ← *3s*) transitions. Duncan and coworkers[1–4] and Beyer and coworkers[5–7] have measured photodissociation of solvated $Mg^+$ complexes such as $Mg^+(H_2O)_n$ and $Mg^+(CO_2)_n$ obtaining detailed information on photochemical pathways, geometries, and spectroscopic parameters in these systems. In parallel, other groups have focused on complexes of $Mg^+$ with various organic molecules,[8–18] with photoinitiated C-H activation by $Mg^+$ reported in certain cases.

Although they do not observe C-H activation, Misaizu and co-workers report several other interesting photodissociation pathways in their studies of $Mg^+$ - $XCH_3$ complexes (X = F, Cl, Br, I).[12,13,15,16] In photolysis of $Mg^+(ICH_3)$ from 24000 to 44000 $cm^{-1}$, for example, the authors observe energy-dependent competition between reaction products where the charge is retained on the metal ($Mg^+$, $MgI^+$) and ones where charge transfer occurs to the non-metal fragment ($I^+$, $ICH_3^+$).[12] In later studies, in addition to mass spectrometrically detecting the charged products, they measured photofragment images,[19,20] allowing them to determine the fragment anisotropy and kinetic energy release (KER).[21–23] For linear molecules, $\Delta\Lambda=0$ transitions lead to parallel anisotropy ($\beta=2$ to 0) and $\Delta\Lambda=\pm1$ are perpendicular ($\beta=-1$ to 0), with values near 2 and –1 corresponding to dissociation occurring faster than a rotational period. However, the Mg-I-C bond angle in $Mg^+$-$ICH_3$ is calculated[20] to be 101°, so interpretation of the anisotropy is not as straightforward as it is for a linear molecule. Perpendicular anisotropy is observed in images of $MgI^+$ fragments at 266 nm, revealing that the transition dipole moment is perpendicular to the dissociation axis (roughly the I – $CH_3$ bond axis) and parallel to the Mg – I bond axis.[20] This indicates that photodissociation occurs via promotion of the Mg 3*s* electron to a 3*p* orbital aligned with the Mg-I bond.

Measurement of KER from a fragment image reveals how energy is distributed to the photofragments at a particular photolysis energy (hν):

$$h\nu + E_{int}(AB^+) = D_0(A^+\text{-}B) + KER + E_{int}(A^+) + E_{int}(B) \qquad (1)$$

If the ions start internally cold ($E_{int}(AB^+)=0$), then the maximum kinetic energy release gives an upper bound to the bond dissociation energy ($D_0(A^+\text{-}B)$). In small systems, there are few possible quantum states for the fragments, so a significant fraction are likely to be formed in their ground states. In this case, measuring the KER can give very precise bond strengths. In addition, the observed values of the KER can determine the electronic,[24] spin-orbit[25] and vibrational[26] states of the photofragments ($E_{int}(A^+)$, $E_{int}(B)$). In some cases, photofragment imaging reveals that the ions have more energy than expected – that is, they are *not* internally cold immediately prior to photodissociation. This can be due to hot ions ($E_{int}(AB^+)>0$), in which case the measured KER can give information on low-lying vibrationally[27] or electronically excited states.[25] It can also be due to absorption of more than one photon, as in resonance enhanced photodissociation (REPD). This process is suggested to be responsible for the observed photodissociation spectra of ions such as $Mg^+(H_2O)$, $Ca^+(H_2O)$ and $Mn^+(H_2O)$[1,28,29] in which one photon is absorbed via a strong electronic transition to form an excited state whose predissociation lifetime is much longer than its fluorescence lifetime. Absorption of a second photon then leads to the observed photodissociation.

Although small linear molecules are well-suited to imaging experiments, diatomic molecules are the ideal candidates. Magnesium halides and isoelectronic group 13 metal-containing ions are of interest in fundamental physics research such as laser cooling and quantum computing,[30–32] and happen to possess excellent kinematics for imaging. Although neutral MgI has been extensively characterized via electronic[33–35] and rotational[36] spectroscopy, there have been no previous experimental studies of the cation. Recently, Korek and coworkers published the first extensive theoretical study of this molecule, performing high-level *ab initio* multi-reference configuration interaction (MRCI) calculations on $MgI^+$ and other magnesium halide cations to determine their electronic structures and transition dipole moments from their ground electronic states.[37] Further work to understand the fundamental properties of $MgI^+$, including measurement of its bond energy, electronic spectrum and fragmentation pathways, may help inform on the dynamics in photoinitiated intra-cluster reactions observed in metal ion – organic halide complexes. In this work, we report calculated MRCI potential energy curves, photodissociation spectra and photofragment images for visible and UV photodissociation of $MgI^+$.

## II. Methods

The home-built reflectron time-of-flight mass spectrometer/photofragment imaging instrument used in these studies is described in detail elsewhere.[26] This section gives a brief overview of the instrument and provides a description of the $MgI^+$ photofragment spectroscopy and imaging experiments. Magnesium iodide cations are formed by reacting $Mg^+$ with $CH_3I$ in a laser ablation ion source. In the ion source, the second harmonic of a Continuum Minilite II Nd:YAG laser is focused onto a rotating magnesium disk in the presence of a gas mixture of $CH_3I$ in He. The $CH_3I$/He mix is formed by flowing He over a reservoir of $CH_3I$ (*l*) (Alfa Aesar, 99%, stabilized with copper), and is introduced into the source via a pulsed valve (Parker Series 9). Ions expand into vacuum and are transported by a quadrupole ion guide to a quadrupole ion trap that can be cooled. Prior to their arrival, a pulse of He buffer gas is injected into the ion trap to help thermalize the ions to the trap temperature. Ions are stored for ~55 ms before they are extracted from the trap and accelerated to 1800 V. Ions are then re-referenced to ground potential and mass-selected before entering a reflectron.

Photodissociation spectra are collected by intersecting the ion beam at its turning point in the reflectron with the output of a dye laser (Continuum ND6000) pumped by the second (532 nm) or third (355 nm) harmonic of a Nd:YAG laser (Continuum Powerlite 8020). The $MgI^+$ parent and resulting $Mg^+$ or $I^+$ fragment signals are monitored with a microchannel plate (MCP) detector while scanning the dye laser wavelength. For collecting spectra and images at photon energies of 17000 to 21500 $cm^{-1}$, the fundamental frequency of the dye laser output was used with a fluence of ~80 – 100 $mJ/cm^2$. For spectra and images at photon energies of 33000 to 42000 $cm^{-1}$, the output of the dye laser was frequency-doubled with a fluence of ~10 – 50 $mJ/cm^2$.

In imaging experiments, ions are guided through the reflection (now set to ground potential), through an iris, and into a series of three velocity map imaging (VMI) optics.[21] The output of the dye laser is redirected to intersect the ion beam between the first and second VMI optics, which are simultaneously pulsed to high voltage to focus the photofragments onto a second MCP detector; the third VMI optic is grounded to accelerate the ions and separate the parent and fragment species in time. The MCP detector is coupled to a fast phosphor screen (Photonis) and pulsed to high voltage for the minimum amount of time required to collect the entire fragment ion packet. A CCD camera placed behind the phosphor screen captures the resulting photofragment image, typically for ~20000 to 100000 laser shots. Images are compiled with the NuACQ data

acquisition software.[38] Image analysis is done using the BASEX method[39] and the image anisotropy parameter (β) is calculated using the Polar Onion-Peeling Method.[40]

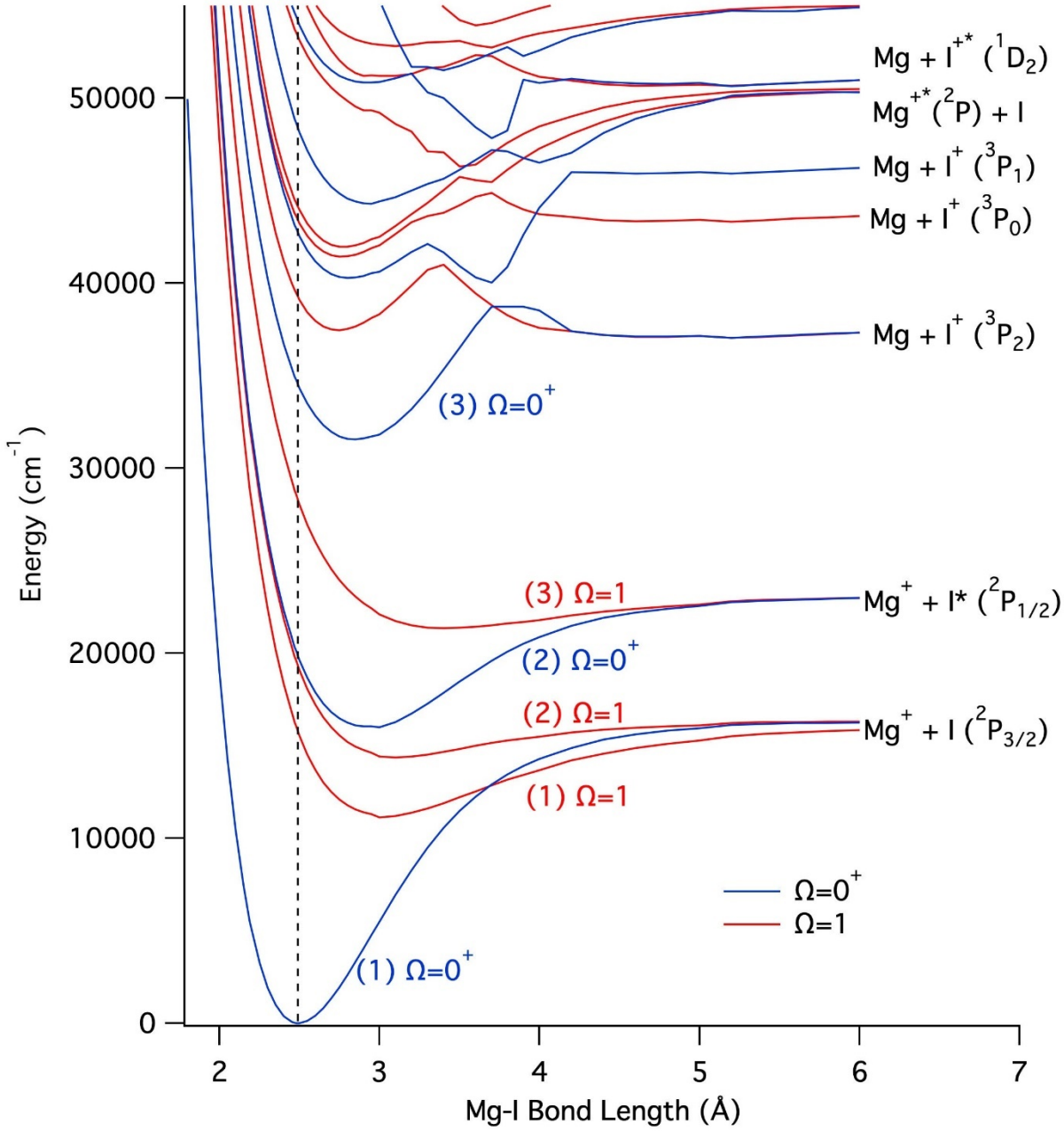


FIG. 1. Potential energy curves for electronic states of $MgI^+$ with $\Omega=0^+$ and 1 and $T_e$ values below 55000 $cm^{-1}$ calculated at the MRCI level with spin-orbit corrections and with the cc-pVTZ basis set. Vertical transition at 2.49 Å is shown with a dashed black line.

## III. Results
### A. Electronic Structure Calculations

Korek and co-workers recently carried out high level multi-reference configuration interaction with Davidson correction (MRCI+Q) calculations on $MgI^+$ as well as on other magnesium monohalides, calculating potential energy curves and transition dipole moment curves for many electronic states, and deriving the corresponding spectroscopic constants.[37] They report a $^1\Sigma^+$ ground state with $D_e$ = 205.8 kJ/mol and $r_e$=2.478 Å and calculate ten singlet and twelve triplet excited electronic states. They also calculated transition dipole moments for transitions to several excited states: the $1^1\Pi$ ($T_e$=12653 $cm^{-1}$, $\mu_{fi}$=0.5 a.u.), 2 $^1\Sigma^+$ (31740 $cm^{-1}$, 1.3 a.u.), 3 $^1\Sigma^+$ (43104 $cm^{-1}$, 1.8 a.u.), and 2 $^1\Pi$ (46096 $cm^{-1}$, 0.2 a.u.). We also carried out MRCI calculations on $MgI^+$ using the Molpro program[41,42] and extended the study of Korek and co-workers by including spin-orbit effects, which are large for $MgI^+$ and significantly affect many of the excited states. Details on the calculations are in the SI. States are labeled by the total angular momentum along the internuclear axis, Ω. Inclusion of spin-orbit effects has negligible effect on the ground state, which is the (1) $\Omega=0^+$ state. It is 99% composed of the $^1\Sigma^+$ state and has $r_e$=2.49 A. Electronic transitions from the ground state are optically allowed (one-photon) to states with $\Omega=0^+$ (parallel) and Ω=1 (perpendicular). Spectroscopic parameters for these states are listed in Table S1 and the potentials are displayed in Figure 1. The excited states have longer bonds and lower vibrational frequencies than the ground state. It is noteworthy that inclusion of spin-orbit effects not only shifts the positions of excited states, but also makes previously forbidden transitions optically allowed. For example, transitions to the (2) $0^+$ and (4) $0^+$ states are predicted to be quite intense, although they are primarily comprised of the (1) $^3\Pi$ and (1) $^3\Sigma^+$ states, respectively. Table S2 summarizes the properties of states with $\Omega=0^-$, 2 and 3 and their potentials are shown in Figure S1. While there are few electronic states below 30000 $cm^{-1}$, there are numerous states at higher energy, which leads to many avoided crossings at energies above ~38000 $cm^{-1}$ and at bond lengths of 3-4 Å. This is due to the presence of several product channels, $Mg + I^+$ ($^3P_{0,1,2}$), $Mg^+$* ($^2P_{1/2,3/2}$) + I ($^2P_{3/2}$) and Mg + $I^+$* ($^1D_2$), at calculated energies of 37000-52000 $cm^{-1}$. The excited states will be discussed in more detail in conjunction with the experimental results.

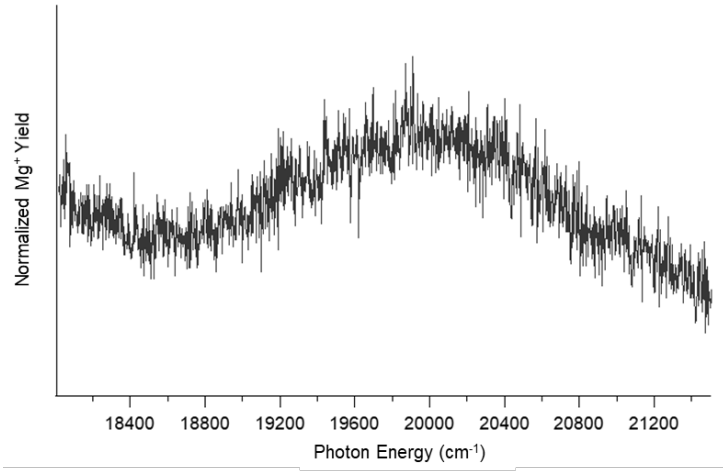


FIG. 2. Photodissociation spectrum of $MgI^+ \rightarrow Mg^+ + I$ from 18000 to 21500 $cm^{-1}$. The spectrum was recorded after cooling the parent ion packet with He trap gas at a nominal trap temperature of 200 K.

**B. $MgI^+ \rightarrow Mg^+ + I$ Photodissociation**

***1. $MgI^+ \rightarrow Mg^+ + I$ Photodissociation Spectrum***. From 18000 to 21500 $cm^{-1}$, slightly above the MRCI predicted bond dissociation energy, $MgI^+$ photodissociates to form $Mg^+ + I$ fragments. Spectra are measured by scanning the photolysis laser while monitoring the $Mg^+$ fragment signal. The spectrum (Figure 2) shows a broad peak centered at ~20000 $cm^{-1}$ with little to no structure, suggesting rapid dissociation from an unbound excited state. Figure 1 shows three optically accessible excited states from the ground (1) $\Omega=0^+$ state in this region. The (1) $\Omega=1$ and (2) $\Omega=1$ states are weakly bound and correlate to ground state products, while the (2) $\Omega=0^+$ state has a deeper well and correlates to ground state $Mg^+$ and spin-orbit excited iodine (I*, $^2P_{1/2}$). The breadth of the spectrum in this region is consistent with direct dissociation following absorption to the repulsive inner wall of the (1) $\Omega=1$ and (2) $\Omega=1$ states. These states have long Mg-I bonds and are formed by strong mixing of the $\Omega=1$ components of the (1) $^3\Pi$ and (1) $^1\Pi$ states. A less likely pathway is absorption to the (2) $\Omega=0^+$ state followed by ultrafast intersystem crossing to the $\Omega=1$ states, though this pathway would likely give rise to a more structured spectrum than is observed. The photon energy at the peak of the spectrum (19900 $cm^{-1}$) best corresponds to absorption to the (2) $\Omega=1$ state, at a vertical energy of 19330 $cm^{-1}$ in our calculations, while transitions to the (1) $\Omega=1$ state contribute more at lower energy.

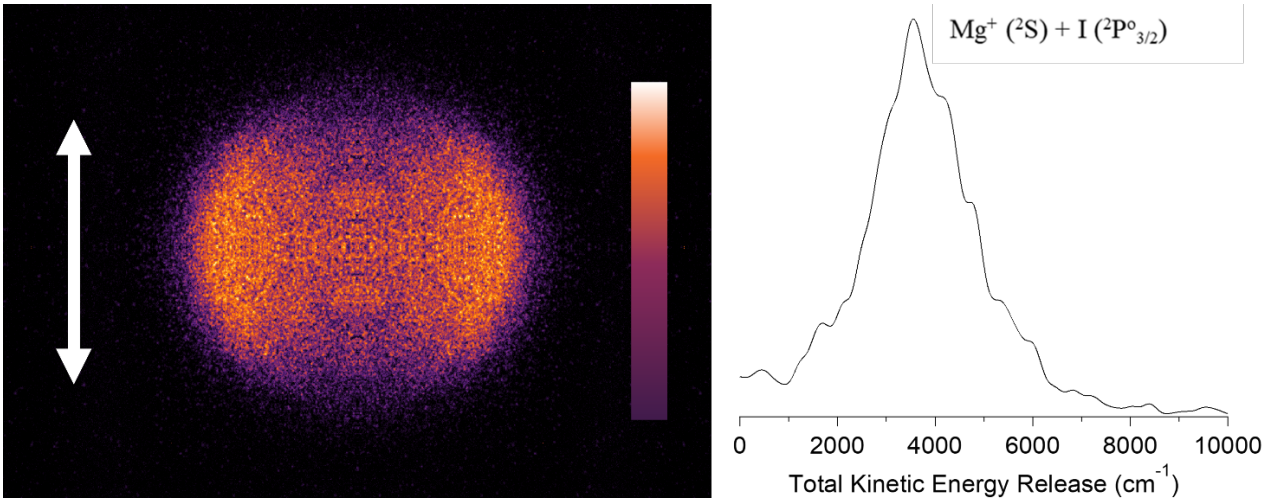


FIG. 3. Photofragment image of $Mg^+$ fragments resulting from photodissociation of $MgI^+$ at 20619 $cm^{-1}$ and corresponding total KER distribution. The image was collected after cooling the ion packet with He trap gas at a nominal trap temperature of 298 K. The image has been top/bottom and left/right symmetrized. Laser polarization is vertical. Color scale bar shown on the right side the image. The lightest colored regions have the highest fragment counts.

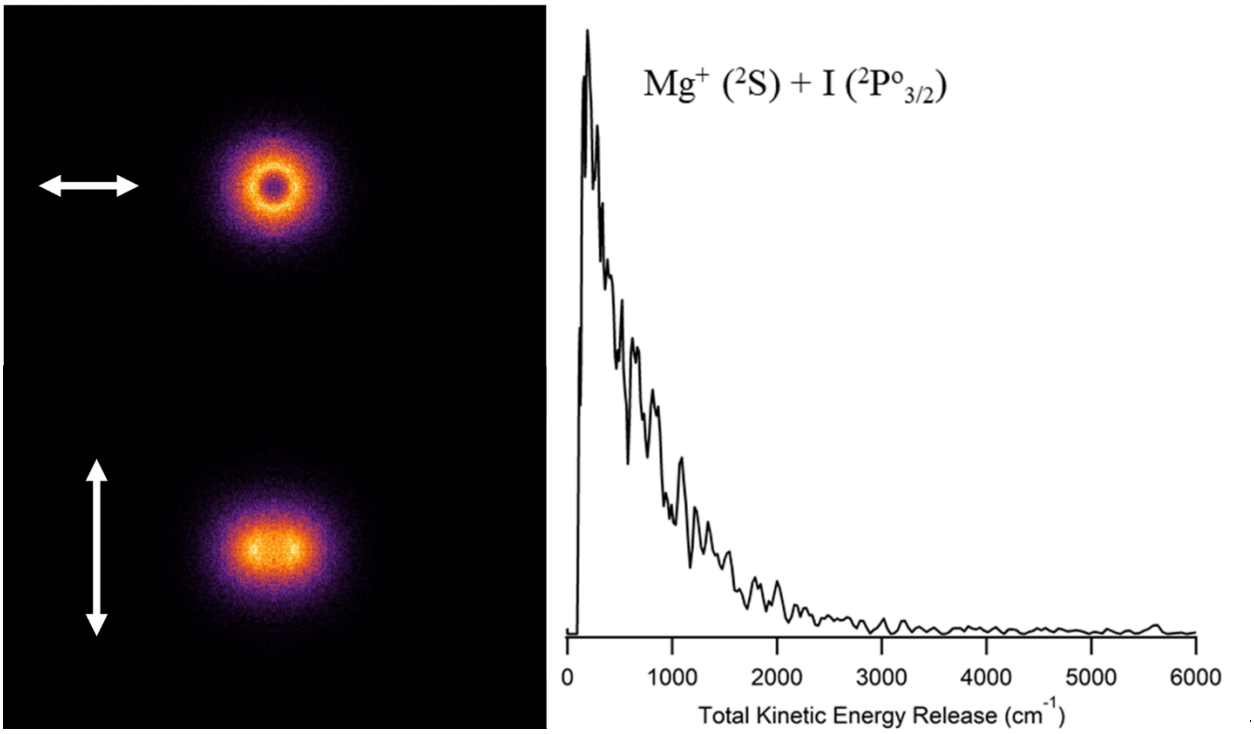


FIG. 4. Photofragment images of $Mg^+$ fragments resulting from photodissociation of $MgI^+$ at 17152 $cm^{-1}$ with laser polarization horizontal (top) and vertical (bottom), and total KER distribution (right) from the image collected using horizontally polarized light. The image was collected after cooling the ion packet with He trap gas at a nominal trap temperature of 200 K. The images shown have been top/bottom and left/right symmetrized.

***2. Images of $Mg^+$ Fragments.*** Photofragment images were taken by tuning the photolysis laser to selected wavelengths along the photodissociation spectrum and gating on the $Mg^+$ fragment at the imaging detector. Figure 3 shows a photofragment image taken near the broad peak of the spectrum in Figure 2. The fragment distribution shows clear horizontal anisotropy ($\beta = -0.7$), consistent with the perpendicular (2) $\Omega=1 \leftarrow$ (1) $\Omega=0^+$ transition predicted in this region. The kinetic energy release (KER) distribution indicates formation of ground state products with moderate KER, giving a rough estimate of $D_0(MgI^+)$. The precision of this value is limited by the rather large FWHM of the peak. Although the experimental conditions used in collection of the image (ion trap temperature = 298 K) certainly contribute to the large FWHM, high fragment KER likely plays a larger role, due to the spot size of the ion beam at the detector, as discussed previously in detail.[26] Since the KER associated with a given pixel increases with the square of the distance (radius) between the pixel and the center of the image, any uncertainty in the KER is magnified as the KER increases. Thus, maximal precision is obtained from images at photon energies as close to a product threshold (atomic state dissociation limit) as possible, with decreasing precision further above threshold. Accordingly, to improve precision, additional images were taken at lower excitation energy (Figure 4). These images show ground state products with very low KER, giving a $D_0$ measurement with excellent precision (203 ± 1.8 kJ/mol, 17000 ± 150 $cm^{-1}$). It is important to note this value and associated uncertainty is based solely on the KER distribution and associated (±) half width at half maximum (HWHM) in Fig. 4. Perpendicular anisotropy ($\beta = -0.6$) suggests that the (1) $\Omega=1 \leftarrow$ (1) $\Omega=0^+$ transition is involved near the dissociation threshold, with a similar excited state lifetime as at higher energies. Image anisotropy also indicates that the parallel (2) $\Omega=0^+ \leftarrow$ (1) $\Omega=0^+$ transition does not contribute significantly to the photodissociation spectrum. However, the (2) $\Omega=0^+ \leftarrow$ (1) $\Omega=0^+$ transition likely results in strong absorption without photodissociation, since it is predicted to be more intense than the (1) $\Omega=1 \leftarrow$ (1) $\Omega=0^+$ transition.

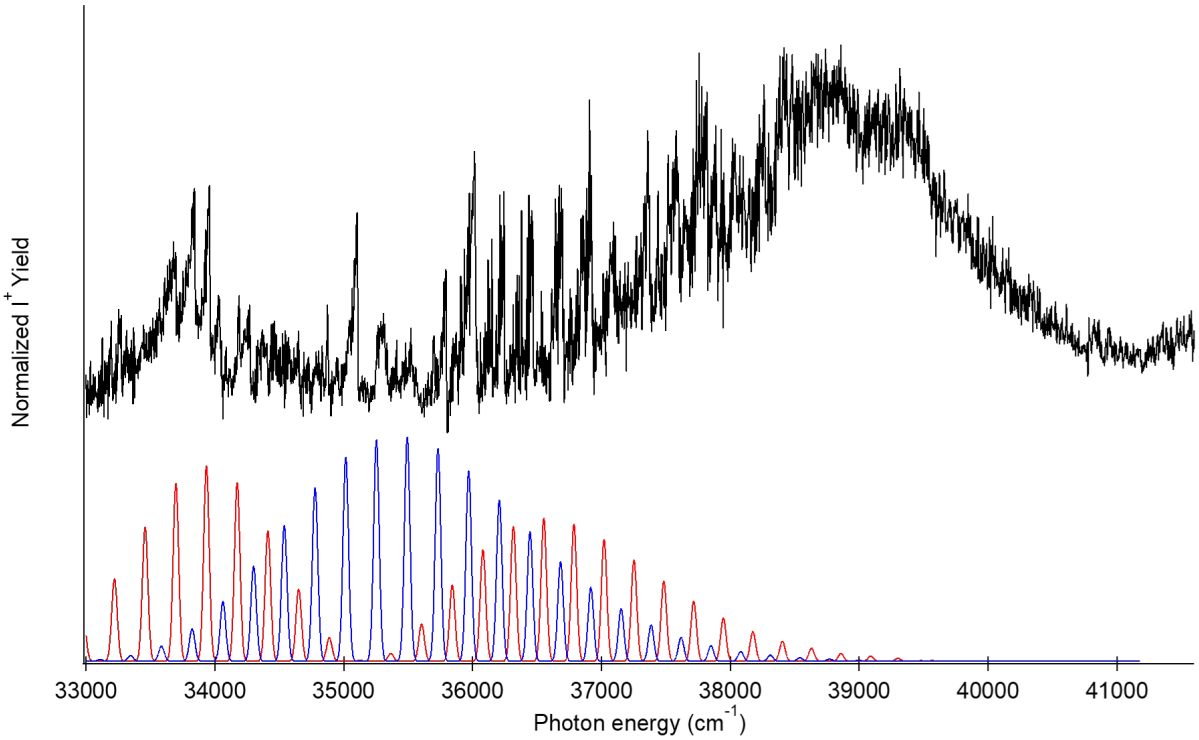


FIG. 5. Photodissociation spectra of $MgI^+ \rightarrow I^+ + Mg$ from 33000 to 40000 $cm^{-1}$. Simulated spectra of the (3) $\Omega=0^+ \leftarrow$ (1) $\Omega=0^+$ from the ground (blue) and first excited (red) vibrational state of the (1) $\Omega=0^+$ state are shown under the experimental spectra (black). Simulated spectra are shifted higher in energy by 1180 $cm^{-1}$ and peaks are shown as 50 $cm^{-1}$ FWHM Gaussians.

### C. $MgI^{+*} \rightarrow I^+ + Mg$ Photodissociation

***1. $MgI^+ \rightarrow I^+ + Mg$ Photodissociation Spectrum.*** In order to probe dissociation dynamics in the higher energy region of the potential energy surfaces of $MgI^+$, the photodissociation spectrum was measured from 33000 to 41000 $cm^{-1}$ (Figure 5). As $D_0(MgI^+)$ = 17000 $cm^{-1}$ and the ionization energy of I exceeds that of Mg by 22624 $cm^{-1}$, only formation of $Mg^+ + I$ is expected from 33000 to 39600 $cm^{-1}$; above 39600 $cm^{-1}$, both $Mg^+ + I$ and $Mg + I^+$ channels are predicted to be active. Surprisingly, exclusively $I^+$ photofragments are formed over this entire range of the spectrum. One possible explanation for this observation is (a) that a significant portion of the parent ions are in a

long-lived excited electronic state prior to photolysis; an electronic state above the threshold for $I^+$ is accessed by UV excitation from this lower-lying excited state, leading to $I^+$ + Mg products. A second possibility is (b) that $I^+$ photofragments are formed via a two-photon process, resonance enhanced photodissociation (REPD), in which absorption of one photon produces $MgI^+$ in a long-lived excited electronic state; these excited molecules then absorb a second photon and dissociate to form Mg + $I^+$. Since analysis of photofragment images of $MgI^+$ (discussed in detail in section C2) overwhelmingly points to (b) as the mechanism for photolysis in the UV, the discussion below assumes the spectrum arises entirely from photolysis of ground ((1) $\Omega = 0^+$) state $MgI^+$.

The $MgI^+ \rightarrow I^+ + Mg$ photodissociation spectrum (Figure 5) from 33000 to 38500 $cm^{-1}$ is highly structured with two underlying broad features, centered at 33800 and 38800 $cm^{-1}$. The spacing of peaks between 33000 and 35500 $cm^{-1}$ is more irregular than the rest of the structured part of the spectrum, with a minimum of ~80 $cm^{-1}$ and a maximum of ~230 $cm^{-1}$. There are ~10 major peaks between 35500 and 38500 $cm^{-1}$ that are consistent with a regular vibrational progression; these are spaced by an average of 227 $cm^{-1}$. The peaks in this region generally become broader with increasing photon energy, and above 38500 $cm^{-1}$ the spectrum is unstructured. Calculated potential energy curves for $MgI^+$ (Figure 1) show allowed transitions to two excited states from the (1) $\Omega=0^+$ ground state in the region of the measured UV photodissociation spectrum (33000 to 41000 $cm^{-1}$). A parallel transition to the (3) $\Omega=0^+$ state with $T_0$ = 31552 $cm^{-1}$ is predicted at a vertical transition energy of 34535 $cm^{-1}$ while a perpendicular transition to the (4) $\Omega=1$ state with $T_0$ = 37401 $cm^{-1}$ is predicted at a vertical transition energy of 39280 $cm^{-1}$ (Table S1). The (3) $\Omega=0^+ \leftarrow$ (1) $\Omega=0^+$ transition should be far more intense ($f$ = 0.197) than the (4) $\Omega=1 \leftarrow$ (1) $\Omega=0^+$ ($f = 7.6 \times 10^{-4}$); the vibrational frequency ($\omega_e$ = 218 $cm^{-1}$) of the (3) $\Omega=0^+$ is also more consistent with the experimental spectrum ($\omega$ = 227 $cm^{-1}$) than that of the (4) $\Omega=1$ ($\omega_e$ = 267 $cm^{-1}$) (Table S1). A Franck-Condon simulated spectrum for the (3) $\Omega=0^+ \leftarrow$ (1) $\Omega=0^+$ transition from both $\nu$=0 (blue dash) and $\nu$=1 (red dash) in the ground electronic state is shown below the experimental spectrum in Figure 5; intensities are calculated assuming equal populations in $\nu''$=0 and $\nu''$=1. Simulated spectra imply most peaks between 33000 and 34000 $cm^{-1}$ and between 37000 and 38500 $cm^{-1}$ come from $\nu''$=1, and most peaks between 35000 and 36000 $cm^{-1}$ come from $\nu''$=0; between 34000 and 35000, and 36000 and 37000 $cm^{-1}$, peaks come from both vibrational levels. The simulation is of the one-

photon absorption spectrum. The observed intensities in the photodissociation spectrum would also be affected by the cross section for absorption of a second photon and by the subsequent photodissociation yield.

The one-photon absorption spectrum of $MgI^+$ from 33000 to 38500 $cm^{-1}$ is expected to be far more intense overall than the region above 38500 $cm^{-1}$; it is worth noting that this is the opposite of what is observed in the photodissociation spectrum. The broad feature centered at 38800 $cm^{-1}$ has the highest intensity in the spectrum. This feature lines up very closely with the energy of the barrier to dissociation of the (3) $\Omega=0^+$ state at r = 3.8 Å (Figure 1). It is therefore possible that this peak arises from both two-photon dissociation of $MgI^+$ and one-photon dissociation of vibrationally hot $MgI^+$. In fact, increasing favorability of the one-photon process with increasing photon energy is consistent with the broadening of the spectrum, as direct dissociation is accessible once the barrier of the (3) $\Omega=0^+$ is overcome energetically. The higher efficiency of one-photon rather than two-photon dissociation also explains the increase in intensity.

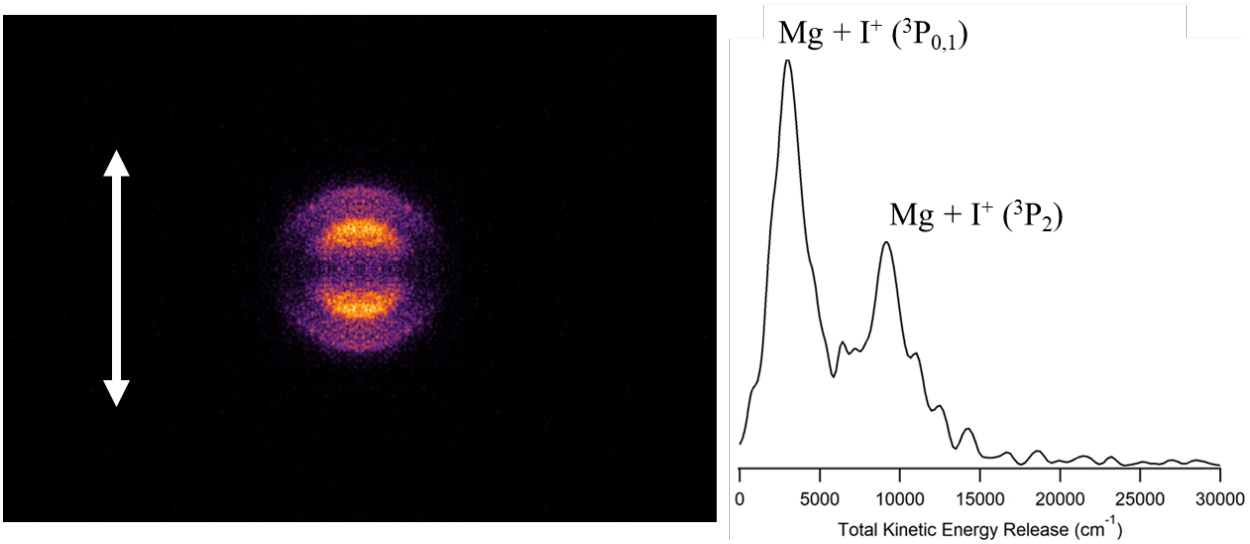


FIG. 6. Photofragment image of $I^+$ fragments resulting from resonance enhanced photodissociation of $MgI^+$ at a one-photon energy of 36245 $cm^{-1}$ and corresponding total KER distribution. The image shown has been top/bottom and left/right symmetrized. Laser polarization is vertical.

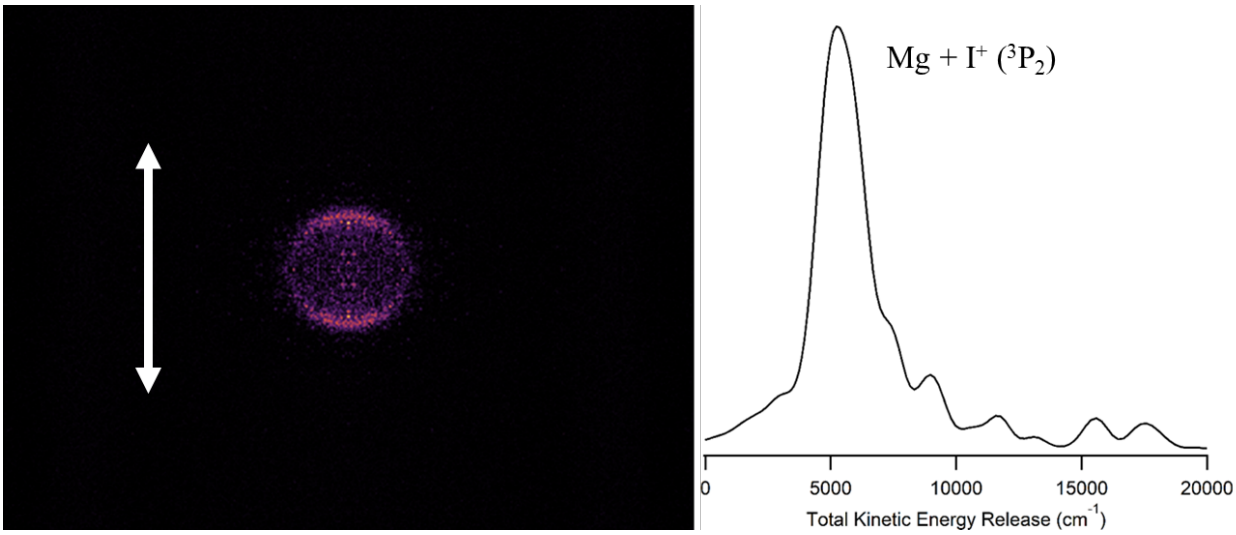


FIG. 7. Photofragment images of $I^+$ fragments resulting from resonance enhanced photodissociation of $MgI^+$ at a one-photon energy of 33835 $cm^{-1}$ and corresponding total KER distribution. The image shown has been top/bottom and left/right symmetrized. Laser polarization is vertical.

***2. Images of $I^+$ Fragments.*** Photofragment images of $I^+$ were collected by gating on the $I^+$ fragment and tuning the ion optics voltages for optimal resolution. As the heavier fragment is imaged, the kinematics are much less favorable than when detecting $Mg^+$, leading to poorer kinetic energy resolution. Figure 6 shows an $I^+$ photofragment image taken at 36245 $cm^{-1}$; this photon energy corresponds to a sharp peak in the middle of the structured region of the photodissociation spectrum (Figure 5). The KER distribution has two peaks, at 3300 and 10100 $cm^{-1}$, corresponding to two different Mg + $I^+$ fragment channels. The two lowest atomic states of Mg are separated by 21850 $cm^{-1}$, while the atomic ground state of $I^+$ is split into three spin-orbit levels with relative energies of 0 ($^3P_2$), 6448 ($^3P_0$) and 7087 ($^3P_1$) $cm^{-1}$. The lower energy peak in the KER distribution is thus due to both $^3P_0$ and $^3P_1$ fragments and the higher energy peak is from $^3P_2$ fragments. $I^+$ ($^3P_{0,1}$) fragments are favored over $I^+$ ($^3P_2$) fragments with a branching ratio of 1.4:1. The fragment distribution also shows near-limiting parallel anisotropy (low KER channel, $\beta$=1.3; high KER channel, $\beta$=1.5). Figure 7 shows a photofragment image taken at 33835 $cm^{-1}$, on a sharp feature near the onset of the spectrum. The KER distribution shows a single peak at 5400 $cm^{-1}$. This peak best corresponds to $I^+$ ($^3P_2$) fragments, but there is a significant discrepancy between the observed decrease in KER (4700 $cm^{-1}$) and the decrease in photon energy (2410 $cm^{-1}$) from the image in Figure 6 to the one in Figure 7.

The observed discrepancy in KER between images along with some energy accounting helps determine by which mechanism $I^+$ fragments are formed at photon energies below the threshold for $I^+$ fragments. From conservation of energy,

$$E_{photon} \bullet n_{photon} + E_{int}(MgI^+) = D_0(Mg\text{-}I^+) + KER + E_{int}(fragments) \quad (2)$$

or

$$KER = E_{photon} \bullet n_{photon} + E_{int}(MgI^+) - D_0(Mg\text{-}I^+) - E_{int}(fragments) \quad (3)$$

where $E_{photon}$ is the energy of one photon, $n_{photon}$ is the number of photons absorbed, $E_{int}(MgI^+)$ is the initial internal energy in the $MgI^+$ parent ion and the bond dissociation energy $D_0(Mg\text{-}I^+)$ is 17000 $cm^{-1}$. For fragments with the same internal energy, plotting KER as a function of the photon energy should give a line with slope $n_{photon}$. This analysis was carried out for nine $I^+$ fragment

images, including the two shown in Figures 6 and 7, collected at photon energies for selected peaks in the photodissociation spectrum shown in Figure 5. The results are shown in Figure S2. The best fit line has a slope of 1.97, indicating that the $I^+$ fragments are due to absorption of two photons. The next step is to determine which state of Mg is formed. If the internal energy in the $MgI^+$ parent ion is assumed to be zero, then the internal energy of the fragments is 45400 ± 1500 $cm^{-1}$. Production of ground state Mg + $I^+$ ($^3P_2$) corresponds to fragments with 22624 $cm^{-1}$ of internal energy compared to $Mg^+$ + I, due to the difference in ionization energies of atomic Mg and I. Thus, the Mg and/or $I^+$ fragments are electronically excited. The only excited states with the appropriate energy are the excited $^3P_J$ states of Mg, with energies of 21850 (J=0) to 21911 $cm^{-1}$ (J=2). If these states are formed, then the internal parent energy calculated from the y-intercept of the plot is zero within the uncertainty, indicating dissociation of ground electronic state ions. Thus, photodissociation in the 33600 to 36700 $cm^{-1}$ region is due to resonance-enhanced two photon absorption and leads to Mg* ($^3P_J^\circ$) + $I^+$ ($^3P_J$) products. Since the vibrational spacing ($\omega_e$ = 365 $cm^{-1}$) in the ground state of $MgI^+$ is much smaller than the uncertainty in KER in the $I^+$ images, the images do not, however, aid in determining which peaks in the photodissociation spectrum arise from $v''=0$ or $v''=1$ in the ground state.

In images at photon energies above 37600 $cm^{-1}$, Mg* ($^3P_J^\circ$) + $I^+$ ($^3P_{2,0,1}$) products are still formed at moderate to high KER, but a new low KER channel is also visible. The low KER fragments are consistent with the Mg* ($^3P_J^\circ$) + $I^+$ ($^1D_2$) channel, which is predicted to open at 75210 $cm^{-1}$ (a one photon energy of 37605 $cm^{-1}$). At photon energies above 38610 $cm^{-1}$, images change in appearance dramatically. There is virtually no fragment intensity at moderate or high KER and very high intensity at near-zero KER. In addition, the most probable KER for this channel does not increase with increasing photon energy from 38610 to 39447 $cm^{-1}$ (Figure S3). The channel to form ground state Mg + $I^+$ products opens at an energy of 39600 $cm^{-1}$ relative to the ground state of $MgI^+$, which is higher than the one-photon photolysis energy for these images. However, this channel can be accessed by photodissociation of vibrationally hot ($v''=1,2,3$) $MgI^+$ via a one-photon process; increasing photofragment yield of $MgI^+$ in lower vibrational states with increasing photon energy is also consistent with the constant KER observed in the images from 38610 to 39447 $cm^{-1}$. This analysis implies that a one-photon mechanism is favored over a two-photon mechanism at photon

energies above 38610 $cm^{-1}$ and photodissociation of $MgI^+$ from 38610 to 39447 $cm^{-1}$ is almost exclusively from a relatively small number of vibrationally excited parent ions.

The opportunity to observe REPD in $MgI^+$ is largely due to the very inefficient dissociation of the (3) $\Omega=0^+$ state coupled with its short radiative lifetime of ~6 ns (based on the calculated oscillator strength), which greatly limits the time for indirect dissociation. There are several metal-containing ions in which similar photodissociation dynamics have been observed. For example, we estimate that the photodissociation quantum yield for $Al_2^+$ near 40000 $cm^{-1}$ is only 0.006.[27] The photodissociation yield for $Mg^+(H_2O)$, $Ca^+(H_2O)$ and $Mn^+(H_2O)$ in the UV is much smaller than expected, and the signal is likely due to REPD.[1,28,29,43] In all of these molecules, the electronic transition to the excited state ($p \leftarrow s$ on the metal) is strongly allowed, leading to a short radiative lifetime, the excited state is bound and thus cannot directly dissociate, and non-radiative transitions to lower-lying electronic states are inefficient because there are few excited states at nearby energies. As demonstrated in this work, measuring photofragment KER by imaging can confirm suspected cases of REPD when spectroscopic data are inconclusive or merely suggestive of it.

## IV. Conclusions

From ground state $Mg^+$ ($^2S$) + I ($^2P_{3/2}$) product KER distributions in $MgI^+$ photofragment images near threshold, we report the first experimental measurement of the $Mg^+$-I bond strength ($D_0(MgI^+)$ = 203.0 ± 1.8 kJ/mol; 2.10 ± 0.02 eV). This value is slightly lower than the MRCI+so calculated bond strength ($D_0(MgI^+)$ = 205.8 kJ/mol). Perpendicular anisotropy in the images of the $Mg^+$ ($^2S$) + I ($^2P_{3/2}$) products at photolysis energies between 17152 and 20619 $cm^{-1}$ is consistent with a $\Omega=1 \leftarrow$ (1) $\Omega=0^+$ transition. The calculations indicate absorption to the (1) $\Omega=1$ state is more likely at lower energy, and the (2) $\Omega=1$ at higher energy in this region. Image anisotropy and the breadth of the photofragment spectrum from 17000 to 21500 $cm^{-1}$ reveal that dissociation is prompt following excitation via these transitions. In agreement, the calculations show that vertical transitions from the ground state at these energies are to the excited states' repulsive inner walls.

At higher photon energy, in the UV, $Mg^+$ products with high KER are predicted, with the lowest energy $I^+$ channel predicted to open at 39600 $cm^{-1}$. However, $I^+$ products are formed at photon energies as low as 33000 $cm^{-1}$ and $Mg^+$ products are not observed. Plotting observed KER

versus photon energy for $I^+$ fragment images at photon energies of 33000 to 37000 $cm^{-1}$ yields a line of best fit with a slope of 1.97, indicating that the observed products are due to resonance enhanced two-photon dissociation, where Mg* ($^3P°_J$) + $I^+$ ($^3P_J$) products are formed after absorption of a second photon from a bound excited state in the energy region corresponding to absorption of one photon. The photofragment spectrum of $MgI^+ \rightarrow Mg + I^+$ from 33000 to 37000 $cm^{-1}$ matches well with simulated spectra of the (3) $\Omega=0^+ \leftarrow$ (1) $\Omega=0^+$ transition from the $\nu=0$ and $\nu=1$ levels of the (1) $\Omega=0^+$ state. Above 38500 $cm^{-1}$, the sharp peaks in the spectrum transition to broad features. While below 38000 $cm^{-1}$ images still show significant intensity at moderate and high KER, images above 38600 $cm^{-1}$ show only one channel at low KER. In the latter energy regime, KER does not increase with photon energy. The spectrum and images in this region can be explained by a one-photon dissociation mechanism to form Mg ($^1S$) + $I^+$ ($^3P_2$) following absorption to the same (3) $\Omega=0^+$ state, but possibly from higher vibrational levels of the (1) $\Omega=0^+$ at lower energies and the ground vibrational level at higher energies.

**Supplementary Material**

Description of MRCI calculations on $MgI^+$; calculated spectroscopic parameters of all $\Omega=0^+$ and 1 states of $MgI^+$ with $T_e$ values below 55000 $cm^{-1}$ (Table S1); potential energy curves for the $\Omega=0^-$, 2 and 3 states with $T_e$ values below 55000 $cm^{-1}$ (Figure S1); calculated spectroscopic parameters of all $\Omega=0^-$, 2 and 3 states of $MgI^+$ with $T_e$ values below 55000 $cm^{-1}$ (Table S2); plots of kinetic energy release versus photon energy for images of $I^+$ fragments (Figures S2 and S3).

**Acknowledgements**

Financial support from the National Science Foundation under award no. CHE-1856490 is gratefully acknowledged. The MOLPRO calculations were carried out at the National Energy Research Scientific Computing Center, a DOE Office of Science User Facility supported by the Office of Science of the U.S. Department of Energy under Contract No. DE-AC02-05CH11231.

## AUTHOR DECLARATIONS

### Conflict of Interest

The authors have no conflicts to disclose.

### Author Contributions

**Schuyler Lockwood**: Investigation (lead); Formal analysis (lead); Writing – original draft (lead); Writing – review and editing (supporting). **Ricardo Metz**: Conceptualization (lead); Formal analysis (supporting); Funding acquisition (lead); Writing – original draft (supporting); Writing – review and editing (lead).

## DATA AVAILABILITY

The data that support the findings of this study are available from the corresponding author upon reasonable request.

## References


[1] K.F. Willey, C.S. Yeh, D.L. Robbins, J.S. Pilgrim, and M.A. Duncan, J. Chem. Phys. **97**, 8886 (1992).
[2] C.S. Yeh, K.F. Willey, D.L. Robbins, and M.A. Duncan, Int. J. Mass Spectrom. Ion Proc. **131**, 307 (1994).
[3] C.S. Yeh, K.F. Willey, D.L. Robbins, J.S. Pilgrim, and M.A. Duncan, J. Chem. Phys. **98**, 1867 (1993).
[4] C.S. Yeh, J.S. Pilgrim, K.F. Willey, D.L. Robbins, and M.A. Duncan, Int. Rev. Phys. Chem. **13**, 231 (1994).
[5] M. Ončák, T. Taxer, E. Barwa, C. van der Linde, and M.K. Beyer, J. Chem. Phys. **149**, 044309 (2018).
[6] T. Taxer, M. Ončák, E. Barwa, C. van der Linde, and M.K. Beyer, Faraday Discuss. **217**, 584 (2019).
[7] T.F. Pascher, E. Barwa, C. van der Linde, M.K. Beyer, and M. Ončák, Theor. Chem. Acc. **139**, 127 (2020).
[8] Y.C. Cheng, J. Chen, L.N. Ding, T.H. Wong, and P.D. Kleiber, J. Chem. Phys. **104**, 6452 (1996).
[9] W.Y. Lu and P.D. Kleiber, J. Chem. Phys. **114**, 10288 (2001).
[10] W.Y. Lu, T.H. Wong, Y. Sheng, and P.D. Kleiber, J. Chem. Phys. **117**, 6970 (2002).
[11] W. Guo, H. Liu, and S. Yang, J. Chem. Phys. **117**, 6061 (2002).
[12] A. Furuya, H. Tsunoyama, F. Misaizu, and K. Ohno, Chem. Phys. Lett. **382**, 283 (2003).
[13] F. Misaizu, A. Furuya, H. Tsunoyama, and K. Ohno, Phys. Rev. Lett. **93**, 193401 (2004).
[14] H. Liu, Y. Hu, S. Yang, W. Guo, X. Lu, and L. Zhao, Chem. Eur. J. **11**, 6392 (2005).
[15] A. Furuya, F. Misaizu, and K. Ohno, J. Chem. Phys. **125**, 094309 (2006).
[16] A. Furuya, F. Misaizu, and K. Ohno, J. Chem. Phys. **125**, 094310 (2006).
[17] Y. Hu, H. Liu, and S. Yang, Chem. Phys. **332**, 66 (2007).
[18] P.D. Kleiber, W. Lu, and Y. Abate, Int. J. Mass Spectrom. **269**, 1 (2008).
[19] K. Okutsu, K. Yamazaki, K. Ohshimo, and F. Misaizu, J. Chem. Phys. **146**, 024301 (2017).
[20] K. Okutsu, K. Yamazaki, M. Nakano, K. Ohshimo, and F. Misaizu, J. Phys. Chem. A **122**, 4948 (2018).
[21] A.T.J.B. Eppink and D.H. Parker, Rev. Sci. Instrum. **68**, 3477 (1997).
[22] M.N.R. Ashfold, N.H. Nahler, A.J. Orr-Ewing, O.P.J. Vieuxmaire, R.L. Toomes, T.N. Kitsopoulos, I.A. Garcia, D.A. Chestakov, S.M. Wu, and D.H. Parker, Phys. Chem. Chem. Phys. **8**, 26 (2006).
[23] P.C. Singh, L. Shen, M.H. Kim, and A.G. Suits, Chem. Sci. **1**, 552 (2010).
[24] M.D. Johnston, M.R. Gentry, and R.B. Metz, J. Phys. Chem. A **122**, 8047 (2018).
[25] S.P. Lockwood, T. Chunga, and R.B. Metz, J. Phys. Chem. A **125**, 7425 (2021).
[26] M.D. Johnston, W.L. Pearson III, G. Wang, and R.B. Metz, Rev. Sci. Instrum. **89**, 014102 (2018).
[27] M.D. Johnston, S.P. Lockwood, and R.B. Metz, J. Chem. Phys. **148**, 214307 (2018).
[28] C.T. Scurlock, S.H. Pullins, J.E. Reddic, and M.A. Duncan, J. Chem. Phys. **104**, 4591 (1996).
[29] W.L. Pearson, C. Copeland, A. Kocak, Z. Sallese, and R.B. Metz, J. Chem. Phys. **141**, 204305 (2014).

[30] M. Wan, J. Shao, Y. Gao, D. Huang, J. Yang, Q. Cao, C. Jin, and F. Wang, J. Chem. Phys. **143**, 024302 (2015).
[31] S.Y. Kang, F.G. Kuang, G. Jiang, D.B. Li, Y. Luo, P. Feng-Hui, W. Li-Ping, W.Q. Hu, and Y.C. Shao, J. Phys. B **50**, 105103 (2017).
[32] Q.S. Yang and T. Gao, Spectrochim. Acta A **231**, 118107 (2020).
[33] R. Yamdagni, Curr. Sci. **39**, 34 (1970).
[34] S.N. Puri and H. Mohan, Pramana **4**, 171 (1975).
[35] P. Kierzkowski, R. Lawruszczuk, and A. Kowalski, Chem. Phys. Lett. **225**, 369 (1994).
[36] K.M. Kilchenstein, D.T. Halfen, and L.M. Ziurys, J. Mol. Spectrosc. **339**, 1 (2017).
[37] N. Abu El Kher, N. El-Kork, and M. Korek, ACS Omega **4**, 21741 (2019).
[38] W. Li, S.D. Chambreau, S.A. Lahankar, and A.G. Suits, Rev. Sci. Instrum. **76**, 063106 (2005).
[39] V. Dribinski, A. Ossadtchi, V.A. Mandelshtam, and H. Reisler, Rev. Sci. Instrum. **73**, 2634 (2002).
[40] G.M. Roberts, J.L. Nixon, J. Lecointre, E. Wrede, and J.R.R. Verlet, Rev. Sci. Instrum. **80**, 053104 (2009).
[41] H.J. Werner, P.J. Knowles, G. Knizia, F.R. Manby, and M. Schütz, WIREs Comput. Mol. Sci. **2**, 242 (2012).
[42] H.-J. Werner, P.J. Knowles, G. Knizia, F.R. Manby, M. Schütz, P. Celani, W. Györffy, D. Kats, T. Korona, R. Lindh, A. Mitrushenkov, G. Rauhut, K.R. Shamasundar, T.B. Adler, R.D. Amos, A. Bernhardsson, A. Berning, D.L. Cooper, M.J.O. Deegan, A.J. Dobbyn, F. Eckert, E. Goll, C. Hampel, A. Hesselmann, G. Hetzer, T. Hrenar, G. Jansen, C. Köppl, Y. Liu, A.W. Lloyd, R.A. Mata, A.J. May, S.J. McNicholas, W. Meyer, M.E. Mura, A. Nicklass, D.P. O'Neill, P. Palmieri, D. Peng, K. Pflüger, R. Pitzer, M. Reiher, T. Shiozaki, H. Stoll, A.J. Stone, R. Tarroni, T. Thorsteinsson, and M. Wang, (2015).
[43] M.A. Duncan, private communication.